PARTICLE TECHNOLOGY AND FLUIDIZATION



AICHE JOURNAL

A CFD-DEM study of the solid-like and fluid-like states in the homogeneous fluidization regime of Geldart A particles

Qiang Guo¹ | Alireza Bordbar¹ | Likun Ma² | Yaxiong Yu³ | Shuliang Xu² | Christopher M. Boyce¹ | Mao Ye²

²Dalian National Laboratory for Clean Energy and National Engineering Laboratory for MTO, Dalian Institute of Chemical Physics, Chinese Academy of Sciences, Dalian, China

³School of Chemical Engineering and Technology, Xi'an Jiaotong University, Xi'an, China

Correspondence

Christopher M. Boyce, Department of Chemical Engineering, Columbia University, New York, NY 10027, USA. Email: cmb2302@columbia.edu

Mao Ye, Dalian National Laboratory for Clean Energy and National Engineering Laboratory for MTO, Dalian Institute of Chemical Physics, Chinese Academy of Sciences, Dalian 116023, China

Email: maoye@dicp.ac.cn

Abstract

The mechanisms underlying homogeneous fluidization of Geldart A particles have long been debated. Recent experiments shed fresh insights that both a solid-like and a fluid-like state exist. Herein, 3D computational fluid dynamics-discrete element method simulations with the incorporation of interparticle van der Waals forces were performed for five typical Geldart A particles to investigate the bed structure in the homogeneous fluidization regime. Simulation results reproduce the existence of the solid-like and fluid-like states, showing that in the solid-like state, particles have enduring and strong interparticle van der Waals forces that stabilize the bed to keep the bed stationary; while in the fluid-like state, the interparticle van der Waals forces are dominated by the drag force, and particles show global circulation. Both interparticle van der Waals forces and friction are found to be necessary for the existence of the solid-like state, and increasing the former has an effect to widen the solid-like state.

KEYWORDS

CFD-DEM simulation, Geldart A particles, homogeneous fluidization, interparticle van der Waals forces, solid-like and fluid-like

1 | INTRODUCTION

A typical gas-solid fluidized bed consists of a vertical vessel, a bed of particles, and a porous distributor at the bottom of the bed to feed gas that exerts drag force on the particles. When the superficial gas velocity (U_s) is lower than the minimum fluidization velocity (U_{mf}), the bed is operated in the fixed-bed regime, and the particles in the bed behave solid-like, that is to say, no particle movement can be seen. By increasing U_g above $U_{\rm mf}$, the drag force becomes sufficient to balance the weight of particles, and fluidization occurs. It is well known that fluidization behavior depends much on the physical properties of particles employed. For Geldart B and D particles, the bed bubbles immediately after $U_{\rm mf}$. While for Geldart A particles, there is an interval of homogeneous fluidization regime, which is also called particulate fluidization or nonbubbling expansion regime, between $U_{\rm mf}$ and the minimum bubbling velocity $(U_{\rm mb})^{1}$ For Geldart C particles, which are the smallest particles in the Geldart's classification diagram, the bed fluidizes poorly due to strong interparticle cohesive forces compared to particle gravity.1

The interval of homogeneous fluidization of Geldart A particles is of great relevance: for fundamental research, it is an ideal case to study the instability and the origin of mesoscale structures in fluidized beds²; for industrial applications, it is the optimal regime for particles to flow in the standpipe to ensure smooth circulation of particles in a reactor-regenerator system.3 Therefore, the physical origin of homogeneous fluidization of Geldart A particles has been studied for a long time. 4,5 Some attributed the stability of uniform suspensions in homogeneous fluidization to the effect of interparticle forces. For example, Menon and Durian⁶ measured velocity fluctuations of particles using diffusion-wave spectroscopy to be essentially 0 during homogeneous fluidization, which led them to conclude that the state of homogeneous fluidization is actually solid-like where the enduring contacts make particles stay at rest. Rietema⁷ suggested that the concept of an effective elastic modulus can keep the bed surface stable when the homogeneously fluidized bed is tilted, such that the surface tilts with the bed. Such effective elastic modulus could be related to the mechanical structure induced by the interparticle forces such as

¹Department of Chemical Engineering, Columbia University, New York, New York, USA

cohesion and friction. Conversely, some other researchers sought a purely fluid dynamic explanation. For example, Cody et al. measured the velocity fluctuation of particles using an acoustic shot noise probe, and found that the average velocity fluctuation of particles increases linearly with the square of $U_{\rm g}$, showing a fluid-like behavior. Garg and Pritchett reported in theoretical analysis that the stability of homogeneous fluidization can be predicted by adding a fluid dynamic force to the particle linear momentum balance equation. Batchelor proposed a predictive criterion for stability based on fluid dynamic considerations and showed that the stability can arise from random fluctuations in the particle velocity. The mechanism underlying the homogeneous fluidization has since then become a matter of debate.

Later, by the addition of fumed silica nanoparticles. Valverde and coworkers¹¹⁻¹³ fluidized a commercially available xerographic toner particle with the average diameter of 8.53 µm, making them Geldart C particles. Due to the reduced cohesion between grains by the added nanoparticles, the system exhibited a wide interval of homogeneous fluidization with the ratio of $U_{\rm mb}$ to $U_{\rm mf}$ about 40. Within such a wide interval, the authors found that even during homogeneous fluidization regime, both solid-like and fluid-like states can be distinguished. Very recently, by increasing U_g using a stepwise method and keeping the change in U_s in every adjustment small, Guo et al. 14 experimentally verified that for true Geldart A particles, both solid-like and fluid-like states also exist even though the interval of homogeneous fluidization is much shorter (the ratio of U_{mb} to U_{mf} for typical Geldart A particles is $1-3^{15}$). These observations imply that the stability of homogeneous fluidization may have two distinct origins: one arising from interparticle forces in the solid-like state and one purely from fluid dynamics in the fluid-like state.

However, limitations in the experimental measurements left open questions about the apparent phenomenon:

- 1. Do particles far from the walls and bed surface move in the solid-like homogeneous fluidization state?
- 2. Are interparticle forces necessary for the existence of both the solid-like and fluid-like homogeneous fluidization states?
- 3. How do interparticle forces affect the transition between the solid-like and fluid-like homogeneous fluidization states?
- 4. The effects of particle size and density on $U_{\rm mf}$ and $U_{\rm mb}$ are well understood; how do these particle properties affect the transition velocity between the solid-like and fluid-like homogeneous fluidization states if the ratio of interparticle forces to particle weight is similar?

Question (1) stems from the fact that it is difficult to investigate the particle motion in the interior of a 3D fluidized bed in experiments. Questions (2)–(4) stem from the fact that corresponding experimental work can be challenging because although some progress has been made in adhesive force measurements by extracting roughness parameters from atomic force microscope surface maps in recent years, ^{16,17} obtaining accurate and *in situ* characterizations of interparticle forces still remains a big challenge, let alone precisely tuning the magnitude of interparticle forces.

Herein, we seek to address these questions by conducting computational fluid dynamics-discrete element method (CFD-DEM) simulations, which can readily and directly incorporate realistic particle-particle (and particle-wall) interactions. In such a way, interparticle forces can be either turned off or on and can be tuned to have different magnitudes. In particular, we considered cohesive van der Waals forces as the interparticle forces studied here. Although interparticle forces can also arise from a variety of other sources, such as electrostatic forces, liquid bridging, and sintering, and all these forces may be encountered in fluidized beds, the cohesive van der Waals forces are generally regarded as the main forces that influence the fluidization behavior of Geldart A particles. In fact, the transition from Geldart C to A and A to B particles has been attributed to the relative magnitude of cohesive van der Waals forces as compared to the magnitude of hydrodynamic forces and gravity. 18 To this end, full 3D CFD-DEM simulations with the considerations of van der Waals forces were conducted in this work.

2 | SIMULATION METHOD

2.1 | Model equations

To carry out the CFD-DEM simulations, MFiX,¹⁹ an open-source CFD software developed by the National Energy Technology Laboratory, was used. In CFD-DEM, the hydrodynamics of gas phase is described by the volume-averaged Navier–Stokes equations and computed on an Eulerian grid with the cell volume of V_c:

$$\frac{\partial \left(\varepsilon_{g}\rho_{g}\right)}{\partial t} + \nabla \cdot \left(\varepsilon_{g}\rho_{g}\vec{\mathbf{u}}_{g}\right) = 0 \tag{1}$$

$$\begin{split} \frac{\partial \left(\varepsilon_{\mathbf{g}} \rho_{\mathbf{g}} \vec{\mathbf{u}}_{\mathbf{g}} \right)}{\partial t} + \nabla \cdot \left(\varepsilon_{\mathbf{g}} \rho_{\mathbf{g}} \vec{\mathbf{u}}_{\mathbf{g}} \vec{\mathbf{u}}_{\mathbf{g}} \right) &= -\varepsilon_{\mathbf{g}} \nabla p_{\mathbf{g}} + \nabla \cdot \overline{\vec{\tau}}_{\mathbf{g}} + \varepsilon_{\mathbf{g}} \rho_{\mathbf{g}} \vec{\mathbf{g}} \\ &+ \sum_{p=1}^{N_{p}} \beta \frac{V_{\mathbf{p}}}{V_{\mathbf{c}}} \left(\vec{\mathbf{u}}_{\mathbf{p}} - \vec{\mathbf{u}}_{\mathbf{g}} \right) \end{split} \tag{2}$$

where ε_g , ρ_g , p_g , and \vec{u}_g are the gas-phase void fraction, density, pressure, and local average velocity, respectively, \vec{u}_p is the particle velocity, β is the interphase momentum exchange coefficient, V_p is the volume of a particle, N_p is the total number of particles, and \vec{g} is the gravitational acceleration. Here, the gas flow is treated as compressible, and the gas-phase density is calculated via the equation of state of an ideal gas law:

$$\rho_{\rm g} = \frac{p_{\rm g} M_{\rm g}}{R T_{\rm g}} \tag{3}$$

where $M_{\rm g}$ and $T_{\rm g}$ are the mole weight and temperature of the gas phase, and R is the gas constant. The stress tensor of the gas phase $\bar{\tau}_{\rm g}$ is calculated by assuming a Newtonian fluid:

$$\bar{\bar{\tau}}_{g} = \mu_{g} \left(\nabla \vec{\mathbf{u}}_{g} + \nabla \vec{\mathbf{u}}_{g}^{\mathsf{T}} \right) - \frac{2}{3} \mu_{g} \left(\nabla \cdot \vec{\mathbf{u}}_{g} \right) \bar{\bar{\mathsf{I}}}$$
 (4)

where μ_g is the viscosity of the gas phase and \bar{l} is an identity tensor.

In CFD-DEM, the particulate phase is represented by N_p spherical particles with the diameter of d_p and density of ρ_p . The motion of each particle is described by Newton's second law:

$$\frac{d\vec{\mathbf{x}}_{p}}{dt} = \vec{\mathbf{u}}_{p} \tag{5}$$

$$m_{\rm p} \frac{d\vec{\mathbf{u}}_{\rm p}}{dt} = m_{\rm p} \vec{\mathbf{g}} + \vec{\mathbf{F}}_{\rm c} + \vec{\mathbf{F}}_{\rm vdw} + \vec{\mathbf{F}}_{\rm d} \tag{6}$$

$$I_{p} \frac{d\vec{\omega}_{p}}{dt} = \vec{T}_{p} \tag{7}$$

where m_p is the mass of the particle, \vec{x}_p is the particle position, \vec{F}_c , \vec{F}_{vdw} , and \vec{F}_d are the net contact force due to particle contact with walls and neighboring particles, the net van der Waals forces arising from particle–particle and particle–wall interactions, and the drag force exerted by surrounding gas phase, respectively, I_p is the moment of inertia of the particle, $\vec{\omega}_p$ is the particle angular velocity, and \vec{T}_p is the sum of all torques acting on the particle.

The particle contact force from particle–particle or particle–wall collisions is obtained from a soft-sphere model, in which a linear spring and a dashpot are used to formulate the normal contact force, while a linear spring, a dashpot, and a slider are used to compute the tangential contact force. Five parameters, including the normal and the tangential spring coefficient (k_n and k_t), the normal and the tangential damping coefficient (η_n and η_t), and the friction coefficient (μ), are necessary inputs to calculate the particle contact force. Among these five parameters, the tangential collisional parameters are related to the normal collisional parameters, $^{19,20}_{n}$ wherein $k_t/k_n=2/7$ and $\eta_t/\eta_n=1/2$, and the normal damping coefficient is related to the normal restitution coefficient (e_n). The values for the normal and tangential particle–particle collisional parameters are the same as those for particle–wall collisions.

The interparticle van der Waals forces between two arbitrary spheres, a and b, with the radius of r_a and r_b , are calculated from the model developed by Rumpf²¹:

$$\vec{F}_{vdw,ab} = \frac{Ar_{ab}}{12s^2} \left(\frac{1}{1 + \frac{r_{ab}}{r_{asp}}} + \frac{1}{\left(1 + \frac{r_{asp}}{s}\right)^2} \right)$$
(8)

where A is the Hamaker coefficient, a constant depending on the material properties, s is the distance between the surfaces of the spheres, r_{asp} is the radius of the asperity, and r_{ab} is the average particle radius:

$$r_{ab} = \frac{2r_a r_b}{r_a + r_b} \tag{9}$$

Note that Equation (8) exhibits an apparent numerical singularity when the distance between two spheres approaches 0. To avoid this, a minimum cutoff separation distance (s_{min}) is used, below which the

interparticle van der Waals forces are assumed to be the force experienced at $s_{\rm min}$. Also, it is obvious that van der Waals forces drop rapidly with increasing separation distance. Therefore, a maximum cutoff separation distance ($s_{\rm max}$) is used, beyond which the van der Waals forces are ignored.

The drag force on a particle exerted by the surrounding gas phase is calculated by

$$\vec{\mathbf{F}}_{d} = -\mathbf{V}_{p} \nabla p_{g} + \beta \mathbf{V}_{p} \left(\vec{\mathbf{u}}_{g} - \vec{\mathbf{u}}_{p} \right)$$
 (10)

where the first and the second terms on the right side represent the effects due to pressure gradient and viscosity, respectively. Gidaspow drag law²² is used to calculate the interphase momentum exchange coefficient:

$$\beta = \begin{cases} 150 \frac{(1 - \varepsilon_{g})\mu_{g}}{\varepsilon_{g}d_{p}^{2}} + 1.75 \frac{\rho_{g} \left| \vec{\boldsymbol{u}}_{g} - \vec{\boldsymbol{u}}_{p} \right|}{d_{p}} & \varepsilon_{g} \leq 0.8 \\ \frac{3}{4}C_{D} \frac{\rho_{g} \left| \vec{\boldsymbol{u}}_{g} - \vec{\boldsymbol{u}}_{p} \right| \varepsilon_{g}^{-1.65}}{d_{p}} & \varepsilon_{g} > 0.8 \end{cases}$$

$$(11)$$

$$C_{D} = \begin{cases} 0.44 & \text{Re} > 1000\\ \frac{24}{Re} \left(1 + 0.15Re^{0.687} \right) & \text{Re} \le 1000 \end{cases}$$
 (12)

$$Re = \frac{\rho_{\rm g} \varepsilon_{\rm g} d_{\rm p} \left| \vec{\mathbf{u}}_{\rm g} - \vec{\mathbf{u}}_{\rm p} \right|}{\mu_{\rm o}} \tag{13}$$

where C_D is the drag coefficient and Re is the particle Reynolds number.

2.2 | Input parameters

In CFD-DEM, the motion of each particle is tracked. Therefore, the computing effort to simulate the same fluidized bed size used previously¹⁴ to experimentally verify the existence of the solid-like and fluid-like states for Geldart A particles, which includes over 1 billion particles, is quite expensive, especially in the case that a variety of U_{σ} needs to be studied in this work (see later in Figures 6 and 7). To greatly reduce the computing effort, a small 3D fluidized bed with the width (L_x) of 3 mm, the depth (L_y) of 1.2 mm, and the height (L_z) of 12 mm was simulated. The same bed size has been used by Ye et al.²³ in a CFD-DEM simulation study, and has been proven to be able to capture some typical features in the homogeneous fluidization regime and capture the effects of particle and gas properties on $U_{\rm mf}$ and $U_{\rm mb}$. Furthermore, additional simulations with increasing the bed depth to be the same as the bed width (the number of particles and CFD cells are increased accordingly) do not significantly affect the transition between different states that will be shown in the following.

The simulated gas phase was air at room temperature and atmospheric pressure with a viscosity of 1.8 \times 10⁻⁵ Pa·s and a molar mass

of 28.8 g/mol. The simulated particles had a density of 1290 kg/m³ and a diameter of 75 µm, well within the classification of Geldart A group. The total number of particles simulated was 36,260. A similar CFD-DEM simulation work by Galvin and Benyahia²⁰ that investigated the effect of van der Waals forces on the fluidization of Geldart A particles using MFiX was referenced to set the input parameters associated with the interparticle van der Waals forces and the particle contact force, including the Hamaker coefficient A, radius of asperity r_{asp} , minimum cutoff distance s_{min} , maximum cutoff distance s_{max} , normal spring constant k_n , tangential spring constant k_t , and friction coefficient μ , which have been listed in Table 1. Note that for a specific coefficient, the value was set to be the same between particleparticle and particle-wall interactions. It is also worth noting that evaluation of the interparticle van der Waals forces is sensitive to the radius of asperity r_{asp} , the effect of which, however, is only crudely estimated in the used Rumpf model.²¹ According to the recent measurements using atomic force microscope, r_{asp} is roughly at the order of magnitude of 0.1 µm for Geldart A particles. Furthermore, it was suggested that Geldart A particles with $r_{\rm asp}$ less than 0.01 μm can be essentially treated as smooth, and only when $r_{\rm asp}$ is larger than 0.1 μm, can the surface asperities drastically influence the interparticle van der Waals forces.²⁴ Therefore, r_{asp} was set to 0.1 μ m, following Galvin and Benyahia.²⁰

In the base case, the Hamaker coefficient A and the friction coefficient μ were set to 1×10^{-19} J and 0.2, respectively. To study the effect of the van der Waals forces, in a set of cases, the Hamaker coefficient was changed to 0 J, 1 \times 10⁻²⁰ J, 2 \times 10⁻²⁰ J, 5 \times 10⁻²⁰ J. 2×10^{-19} J, and 5×10^{-19} J from the base case. The friction coeffi cient was changed to 0, 0.1, and 0.3 from the base case to study the effect of friction in the other set of cases. Furthermore, to verify that the existence of the solid-like and fluid-like states in the homogeneous fluidization regime is not a particular case for the particles studied in the base case, four other Geldart A particles with varying particle density or particle size (see later in Table 4) were also studied. In these cases, the Hamaker coefficient was tuned to keep the ratio of the interparticle van der Waals forces to particle weight (defined as cohesive granular bond number, bond number for short, following Ye et al.²³ and Galvin and Benyahia²⁰ to characterize the strength of the interparticle van der Waals forces) in the fixed-bed regime at a similar magnitude to that in the base case. The initial bed height was also kept the same. Therefore, the number of particles is different among the cases with varying particle size. Except these, all other settings were kept the same.

2.3 | Procedure and initial conditions

The initial packed bed was generated by placing the particles uniformly at the sites of a cubic lattice in the bed region between 0 and 5.5 mm from the distributor and then setting $U_{\rm g}$ to a value (2 mm/s) lower than $U_{\rm mf}$, which causes particles to drop. Typically, the particles can settle into a randomly packed state after 0.2 s, after which the bed pressure drop remains a constant and the particles keep

stationary. The state at 0.5 s was then defined as the initial state, where the bed is operated at fixed-bed regime. The average void fraction and bed height of this initial state is 0.42 and 3.8 mm, respectively.

In the CFD-DEM simulations by Ye et al.²³ and Galvin and Benyahia, 20 to speed-up simulations, U_g was linearly increased vs. time to examine the bed hydrodynamics at different $U_{\rm g}$. Such strategy is believed to influence the stability in the bed, as a perturbation in U_g holds for every time step. Also, Wang et al.²⁵ showed that the unreasonable varying trend of $U_{\rm mb}$ with gas-phase viscosity predicted by Ye et al.²³ using the U_g linear-increasing strategy can be corrected by using U_g step-increasing strategy, because the former may produce a delay in the response of bed dynamics. Therefore, in this work, $U_{\rm g}$ was increased step-by-step and the increase of $U_{\rm g}$ in every adjustment was kept small, typically as 0.25 mm/s, similar to that has been used in experiments. 14 The simulations were run for 1.5 s for each $U_{\rm g}$. Such time is sufficient to allow the bed to reach a steady state, as proven from the fluctuation of the bed pressure drop. The data from the last 1 s were used for statistical analysis. Besides the fluidization process, a defluidization process was also performed in the base case, where U_g was decreased from a high value (20 mm/s), in which the bed is strongly bubbling, step-by-step to finally 0 m/s.

3 | RESULTS AND DISCUSSION

This section is organized as follows. First, the simulation results from the base case are analyzed in detail. Then, the transition velocities from cases with different Hamaker coefficients or different friction coefficients from the particles studied in the base case are compared to show the effect of van der Waals forces and friction on the range of $U_{\rm g}$ in which different regimes exist. Finally, the simulation results from cases with four different Geldart A particles are analyzed to show the effect of particle density and particle size.

3.1 | Analysis of the base case

3.1.1 | Gas void fraction and particle velocity

Figures 1 and 2 show the distribution of gas void fraction and particle velocity magnitude at different $U_{\rm g}$ in the fluidization process by increasing $U_{\rm g}$ step-by-step, respectively. Supporting Information Figure S1 shows the equivalent plots to Figure 2, but for the results obtained from the de-fluidization process by decreasing $U_{\rm g}$ step-by-step. The snapshots shown in Figures 1 and 2, and Figure S1 correspond to the instant at t=1.5 s for each $U_{\rm g}$. More intuitive and informative presentations of Figures 1 and 2 are shown as videos in Supporting Information Videos S1 and S2, respectively, in which a collection of 100 snapshots taken in the last 1 s is included at each $U_{\rm g}$. In these plots and videos, along the side of the bed, a ruler in the unit of m is placed to show the change of bed height.

As can be seen from Figures 1 and 2, with the increase of U_g , four different regimes can be clearly distinguished. At $U_g = 3$ and 4 mm/s (panel A), the bed keeps stationary, and the bed height remains constant with the change of U_g from 3 to 4 mm/s, equal to the initial packed bed height. Also, the particle velocity magnitude is essentially 0 m/s. These characteristics indicate that the bed is operated in the fixed-bed regime. At $U_g = 5$ and 6 mm/s (panel B), the bed height begins to expand compared to in the fixed-bed regime, indicating that the bed is already fluidized. With the increase of $U_{\rm g}$ from 5 to 6 mm/s, the bed expansion is also increased. Due to a narrow bed width and a convex parabolic gas velocity profile resulted from a no-slip wall boundary condition (open pipe Re is at the magnitude of 1), the bed surface is changed from nearly flat in the fixed-bed regime to convex at the center in this regime. At the same time, the particle velocity magnitude is still 0 m/s and shows no movement in the video. As a result, the distribution of gas void fraction does not change with time at a specific U_g . A further check indicates that particles in the interior also do not move. This addresses open question (1) mentioned in the Introduction section, confirming that this state is truly solid-like. At $U_g = 8$ and 9 mm/s (panel C), the bed expands further. But different from at $U_g = 5$ and 6 mm/s, the videos of both the gas void fraction and particle velocity magnitude show that the bed is released from a frozen state, and behaves like a fluid, in which particles display global

circulation. From the video of the gas void fraction, it can be seen that some small and short-lived gas voids are formed and moving in the bed. Although looking like gas bubbles, these gas voids should not be identified as bubbles, since (1) these void structures contain much more particles than gas bubbles (the gas void fraction in these gas voids is typically much smaller than 0.8), (2) these void structures disappear quickly, 12,26 and (3) the rupture of these gas voids at the bed surface occurs in a gentle manner, without the capacity of gas bubbles to break through in a manner which makes the bed surface oscillate violently. Upon further increasing $U_{\rm g}$ to 12 and 13 mm/s, clearly recognizable bubbles with a void fraction larger than 0.8 can be seen, and the bubble size increases with increasing $U_{\rm g}$. Furthermore, the rupture of gas bubbles makes the bed surface fluctuate violently. Both characteristics feature naturally in the bubbling fluidization regime.

Overall, the gas void fraction is nearly uniformly distributed in the bed at $U_{\rm g}=5$, 6, 8, and 9 mm/s, and there are no obvious gas bubbles at these values of $U_{\rm g}$. Therefore, the bed should be regarded as being operated in the homogeneous fluidization regime. However, the fluidization characteristics are different between panels B and C in Figures 1 and 2 (or Videos S1 and S2): panel B displays a solid-like behavior, in which the bed remains static, although bed is expanded compared to fixed bed; panel C shows a fluid-like behavior, in which dynamic gas voids and particle movement can be seen. These

TABLE 1 Parameters used in the base case

Quantity	Symbol	Unit	Value
System geometry	$L_x \times L_y \times L_z$	mm	$3 \times 1.2 \times 12$
Number of CFD cells	$N_x \times N_y \times N_z$	-	$12\times5\times48$
Gas temperature	T_g	K	293.15
Gas mole weight	$M_{\rm g}$	g/mol	28.8
Gas viscosity	μ_{g}	Pa·s	1.8×10^{-5}
Gas constant	R	J/(mol K)	8.314
Number of particles	$N_{\rm p}$	-	36,260
Initial bed height (m)	Н _В	mm	3.8
Particle diameter	$d_{\rm p}$	μm	75
Particle density	$ ho_{p}$	kg/m³	1290
Friction coefficient	μ	-	0.2
Hamaker coefficient	Α	J	1×10^{-19}
Radius of asperity	r_{asp}	μm	0.1
Minimum cutoff distance	S _{min}	nm	0.4
Maximum cutoff distance	S _{max}	μm	20
Normal restitution coefficient	e_{n}	-	0.9
Normal spring constant	k _n	N/m	7
Tangential spring constant	k_{t}	N/m	2
CFD inlet boundary condition	-	-	Fixed $U_{\rm g}$
CFD outlet boundary condition	-	-	Atmospheric pressure
CFD wall boundary condition	-	-	No slip
CFD time step	dt_{CFD}	S	1×10^{-5}
DEM time step	dt_{DEM}	S	1×10^{-6}
Gravitational acceleration	$\overset{ ightarrow}{m{g}}$	m/s ²	9.81

observations are in good agreement with those reported in experiments from Valverde et al. 11-13 for modified Geldart C particles and Guo et al. 14 for conventional Geldart A particles. This similarity to experimental results provides confidence that CFD-DEM simulations reproduce the physics of the existence of both the solid-like and fluid-like states in the homogeneous fluidization regime for Geldart A particles, and thus CFD-DEM simulations can provide further insights into the mechanisms underlying these two states. In the following context, the solid-like and the fluid-like state in the homogeneous fluidization will be termed as "solid-like homogeneous fluidization regime" and "uniform nonbubbling fluid-like fluidization regime," respectively, to keep consistent with previous experimental works. 11,14

At the same $U_{\rm g}$ as in Figures 1 and 2, but in the de-fluidization process, the same particle dynamics and bed expansion characteristics in the solid-like homogeneous fluidization regime and uniform nonbubbling fluid-like fluidization regime are also observed, as shown in Figure S1.

Previous researchers have found that for Geldart A particles, gross circulation of particles is displayed in the absence of obvious bubbles. Figure 2C and Video S2C also confirm that particle global circulation prevails in the uniform nonbubbling fluid-like fluidization regime. Furthermore, Figure 3 shows the time-averaged particle velocity field (first row), given by green arrows, in the bed height between 0 and 4.5 mm from the distributor at $U_{\rm g}=8$ and 9 mm/s. Interestingly, a pair of counter-rotating convection rolls of equal size is observed. Such convection pattern is very similar to previously reported wall-driven convective motion in granular

systems under vibration.²⁷ The underlying mechanisms of the convection pattern in Figure 3 should be also induced by wall friction. In addition, the second row in Figure 3 shows that the vertical gas velocity is higher in the middle region than in the near-wall region. These effects make the particles near the bottom move upward from the middle zone while particles near the top of the bed move downward along two sidewalls. Additional simulations increased the bed depth to be the same as the bed width, increasing the number of particles to 95,830. These simulations also show similar patterns in terms of particle convection and vertical gas velocity distribution, as shown in Supporting Information Figure S2. However, as the wall friction effect can be less pronounced in a much larger system, it is anticipated that the particle convection pattern may be changed according to the system size. Furthermore, the system geometry and 2D vs. 3D nature may also play a role. It is noted that the particle convection pattern reported here is different from that reported in a previous 2D CFD-DEM simulation study.²⁸ Nevertheless, these patterns give clear evidence of global circulation of particles in the uniform nonbubbling fluid-like fluidization regime without obvious bubbles.

Although both the modified Geldart C particles^{11–13} and conventional Geldart A particles¹⁴ were experimentally validated to show both the solid-like and fluid-like states in the homogeneous fluidization regime, they show some different characteristics. In particular, the modified Geldart C particles undergo a dynamic aggregation process,^{12,29,30} while for Geldart A particles, it has been questioned for long whether or not aggregates are present in the homogeneous

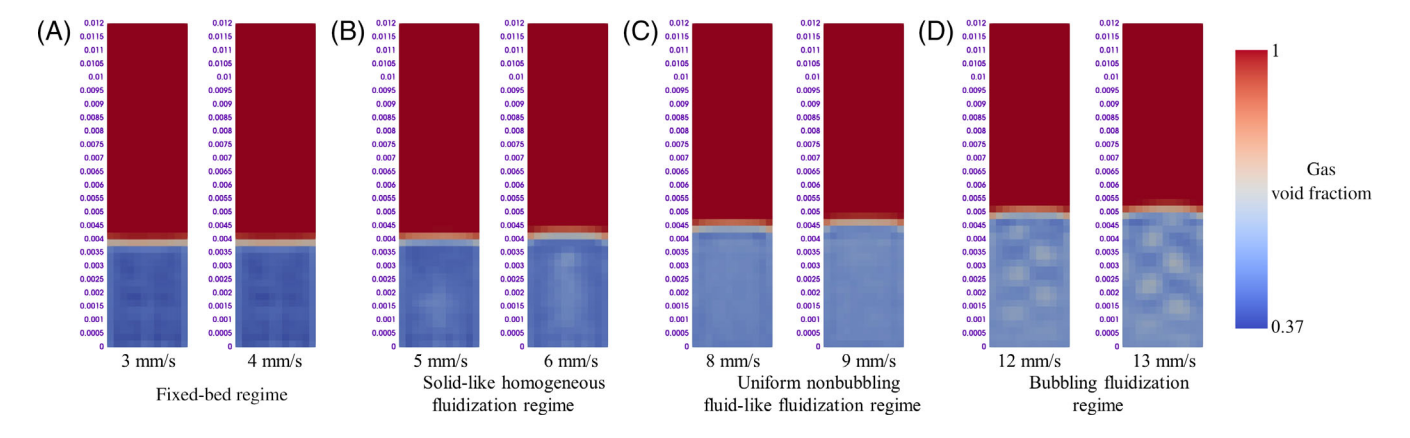


FIGURE 1 Distribution of gas void fraction in the bed at different U_g in the fluidization process

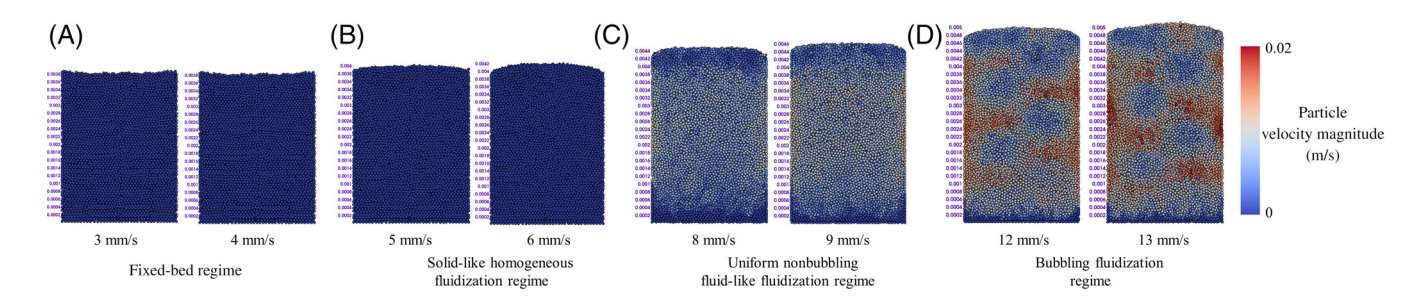


FIGURE 2 Distribution of particle velocity magnitude at different U_g in the fluidization process

fluidization regime. 31,32 By using the sedimentation model originally developed for the modified Geldart C particles, 29,30 Guo et al. 14 estimated that the possible aggregate size in the bed of Geldart A particles is similar to the particles size, that is to say, different from the modified Geldart C particles, Geldart A particles do not display aggregation structures in the homogeneous fluidization regime. From Video S2, it can be seen that indeed the particles fluidize individually in the uniform nonbubbling fluid-like fluidization regime. Furthermore, an inhomogeneity factor based on the scalar variance of particle volume fraction, originally used to characterize the extent of subgrid mesoscale structures in coarse-grained simulations in the field of drag correlation development, 33,34 is introduced to calculate the uniformity of the distribution of particles. The definition of the inhomogeneity factor ($H_{\rm in}$) is shown in Equation 14, where the brackets, $\langle \cdot \rangle$, denote an ensemble average (averaged over all cells below the bed surface).

$$H_{in} = \frac{\sqrt{\left\langle \left[(1 - \varepsilon_g) - \left\langle (1 - \varepsilon_g) \right\rangle \right]^2 \right\rangle}}{\left\langle (1 - \varepsilon_g) \right\rangle} \tag{14}$$

Typically, in a coarse grid, H_{in} takes a value between 0 and 1.³³ A value of 0 implies a homogeneous subgrid structure, and

increasing $H_{\rm in}$ from 0 indicates an increasingly inhomogeneous subgrid structure. By analyzing the time-averaged data for a certain $U_{\rm g}$ in the uniform nonbubbling fluid-like fluidization regime, it is calculated that $H_{\rm in}$ lies around 0.01–0.02 (see Supporting Information - Table S1), demonstrating that particles are uniformly distributed in the bed. As a comparison, $H_{\rm in}$ increases with $U_{\rm g}$ and attain values larger than 0.1 in the bubbling fluidization regime when there are gas bubbles in the bed. The magnitude of $H_{\rm in}$ in the uniform nonbubbling fluid-like fluidization regime does not change significantly within different simulation cases with different Hamaker coefficient, friction coefficient, particle size, or particle density. Therefore, particles are not likely aggregated in the uniform nonbubbling fluid-like fluidization regime, although the interparticle van der Waals forces are turned on (the magnitude of the interparticle van der Waals forces will be discussed in the following).

3.1.2 | Granular temperature

Figure 4 shows the distribution of granular temperature (θ_p), which characterizes particle velocity fluctuations, in the bed at different U_g . The pattern shown in Figure 4 is at the instant of 1.5 s for different U_g

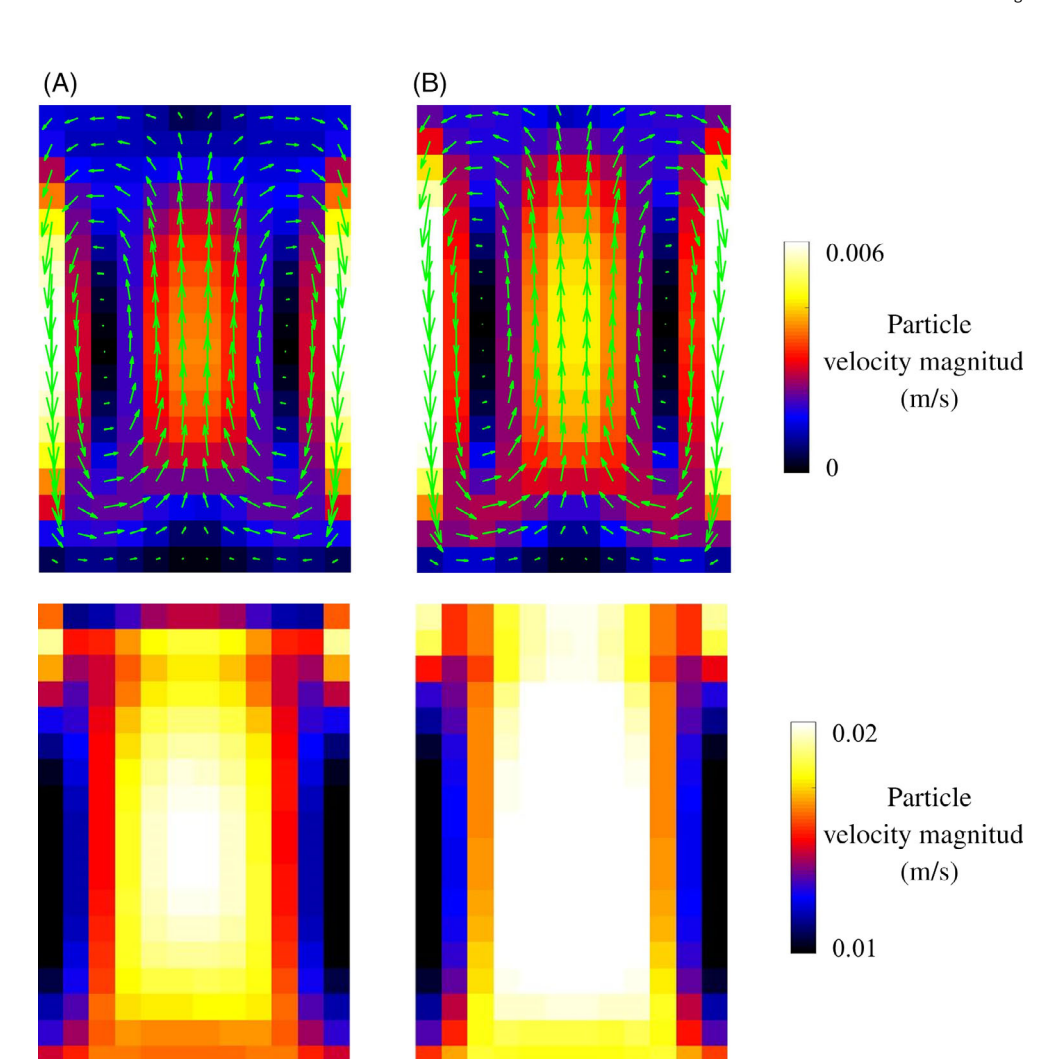


FIGURE 3 (First row) Timeaveraged particle flow field given by green arrows and (second row) time-averaged vertical gas velocity in the uniform nonbubbling fluid-like fluidization regime in the fluidization process: $U_g = (A) 8 \text{ mm/s}$ and (B) 9 mm/s

and is the representative for a certain $U_{\rm g}$. The granular temperature was calculated in each CFD cell as:

$$\theta_{p} = \frac{\theta_{p,x} + \theta_{p,y} + \theta_{p,z}}{3} \tag{15}$$

$$\theta_{p,i} = \left\langle \left(u_{p,i} - \left\langle u_{p,i} \right\rangle \right)^2 \right\rangle \tag{16}$$

Simulation results show that granular temperature is 0 m²/s² in the fixed-bed regime and solid-like homogeneous fluidization regime. This is expected since the particle velocity magnitude is also 0, as shown in Figure 2. In the uniform nonbubbling fluid-like fluidization and bubbling fluidization regimes, granular temperature is larger than 0 and increases with $U_{\rm g}$. These differences further strengthen the separation in flow behavior between the solid-like homogeneous fluidization and uniform nonbubbling fluid-like fluidization regimes. The value of O granular temperature everywhere in the solid-like homogeneous fluidization regime is similar to the experimental measurement results in the homogeneous fluidization regime by Menon and Durian⁶ using diffusing-wave spectroscopy. The nonzero granular temperature that increases with $U_{\rm g}$ in the uniform nonbubbling fluid-like fluidization regime is similar to the experimental measurements using an acoustic shot noise probe by Cody et al.8 These results suggest that previous studies only focused on a certain regime of homogeneous fluidization. A possible reason is that in these studies, although U_g was adjusted step-by-step, the change of $U_{\rm g}$ in every adjustment was relatively large as compared to the previous experiments by Guo et al. 14 and the simulations conducted here. So, these studies may have missed the full spectrum of particle behavior in the homogeneous fluidization regime, which should include both a solid-like and a fluid-like state.

3.1.3 | Force analysis

Figure 5 shows the distribution of the ratio of the interparticle van der Waals forces to particle weight (first row), the ratio of vertical particle drag force to particle weight (second row), and the ratio of vertical interparticle van der Waals forces to vertical drag force (third row) in the bed at the instant of 1.5 s for different $U_{\rm g}$ in the fluidization process, providing a representative snapshot for each value of $U_{\rm g}$. Supporting Information Figure S3 shows the equivalent plots to Figure 5, but for the results obtained in the de-fluidization process. With a Hamaker coefficient of 1×10^{-19} J used in the base case, the bond number is in the range between 0 and 10, with 80% lower than 5.6, similar to the magnitude used in previous CFD-DEM simulations of Geldart A particles. 20,23 Also, such magnitude is in accordance with the postulate that for Geldart A particles, the interparticle van der Waals forces are slightly larger or at the comparable magnitude with particle weight. 1,30,35

It can be seen from Figure 5 and Figure S3 that in the fixed-bed regime, over half number of particles have a bond number around 5, while the vertical drag force of all particles is lower than the particle weight. As a result, the bed keeps stationary and the bed height does

not expand. In the solid-like homogeneous fluidization regime, the distribution of the bond number is similar to that in the fixed-bed regime, which has an effect to stabilize the bed and make the bed stay at rest. At the same time, the vertical drag force of some particles is larger than the particle weight, which has the effect to fluidize the bed. As a result, the bed expands to a higher height, but remains solid-like after reaching a steady state. As compared to the solid-like homogeneous fluidization regime, in the uniform nonbubbling fluid-like fluidization regime more particles have a vertical drag force larger than the particle weight, and the bond number greatly drops with about half of the particles having 0 interparticle van der Waals forces. The decreased interparticle van der Waals forces allow the particles to move, but the magnitude of the drag force is not strong enough to form an obvious bubble. Therefore, the bed displays a fluid-like state with small gas voids. In the bubbling fluidization regime, the interparticle van der Waals forces vanish for most of particles, and the vertical drag force is enhanced. Large bubbles are formed in this regime.

The third row of Figure 5 and Figure S3 shows the ratio of vertical interparticle van der Waals forces to vertical drag force. The results demonstrate that, in the solid-like homogeneous fluidization regime, the vertical interparticle van der Waals forces of most particles are larger than vertical drag force, showing that this state is dominated by the interparticle van der Waals forces, similar to in the fixed-bed regime. In contrast, in the uniform nonbubbling fluid-like fluidization regime, more particles have larger vertical drag force than vertical interparticle van der Waals forces, showing that this state is dominated by the drag force, similar to in the bubbling fluidization regime. This analysis confirms the physical mechanisms proposed in prior experimental studies. 7.9.13,14

3.1.4 | Bed height and pressure drop profiles

Figure 6 shows the bed height and its standard deviation as a function of $U_{\rm g}$ in both the fluidization and de-fluidization processes. The bed height was calculated using a way similar to that has been used by Ye et al. ²⁸ At first, the bed was divided into five subregions along the x (i.e., width) direction. Then, the z (i.e., height) coordinate of the 98th percentile highest particles in each subregion was identified. The average height of all the subregions and averaged over the time in the last 1 s was determined as the bed height at a certain $U_{\rm g}$. Figure 7 shows the bed pressure drop normalized by the particle weight per unit cross-sectional area $(dp_{\rm n})$ and the standard deviation of the bed pressure drop as a function of $U_{\rm g}$ in both the fluidization and the defluidization processes. The marked transition velocities between different regimes in Figures 6 and 7 are identified from visual inspection of the bed in the fluidization process as follows.

The following trends and demarcations are seen for the increasing gas velocity curves: $U_{\rm mf}$ is the first $U_{\rm g}$ at which the bed begins to expand and a significant value of standard deviation in bed height is observed. $U_{\rm mf}$ is also the point when a peak is observed in the pressure drop and the lowest $U_{\rm g}$ at which a significant standard deviation in pressure drop is observed. At $U_{\rm mf}$, the normalized bed pressure

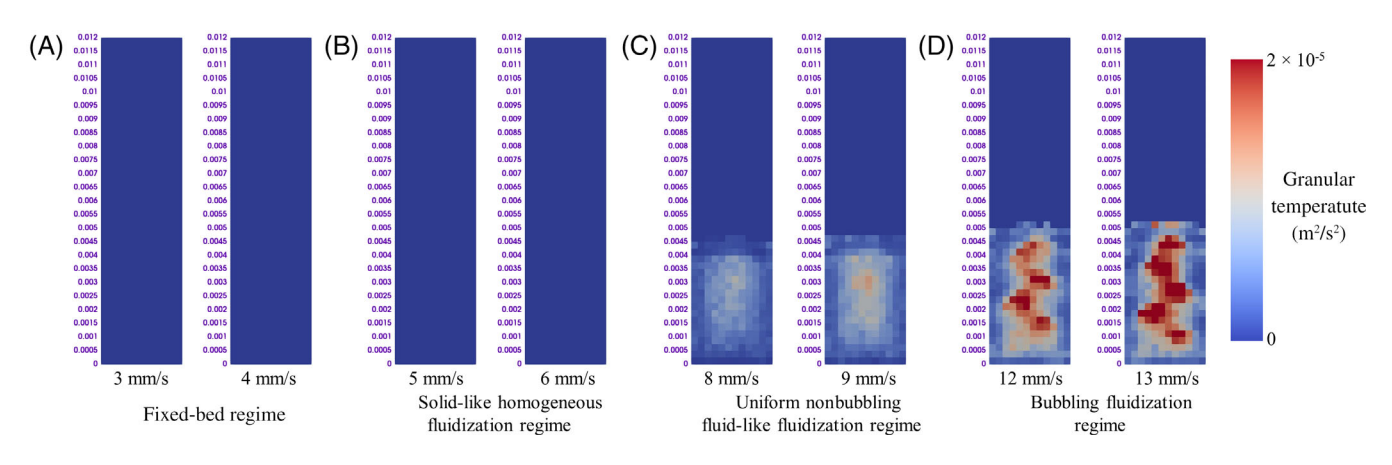


FIGURE 4 Distribution of granular temperature in the bed at different U_g in the fluidization process

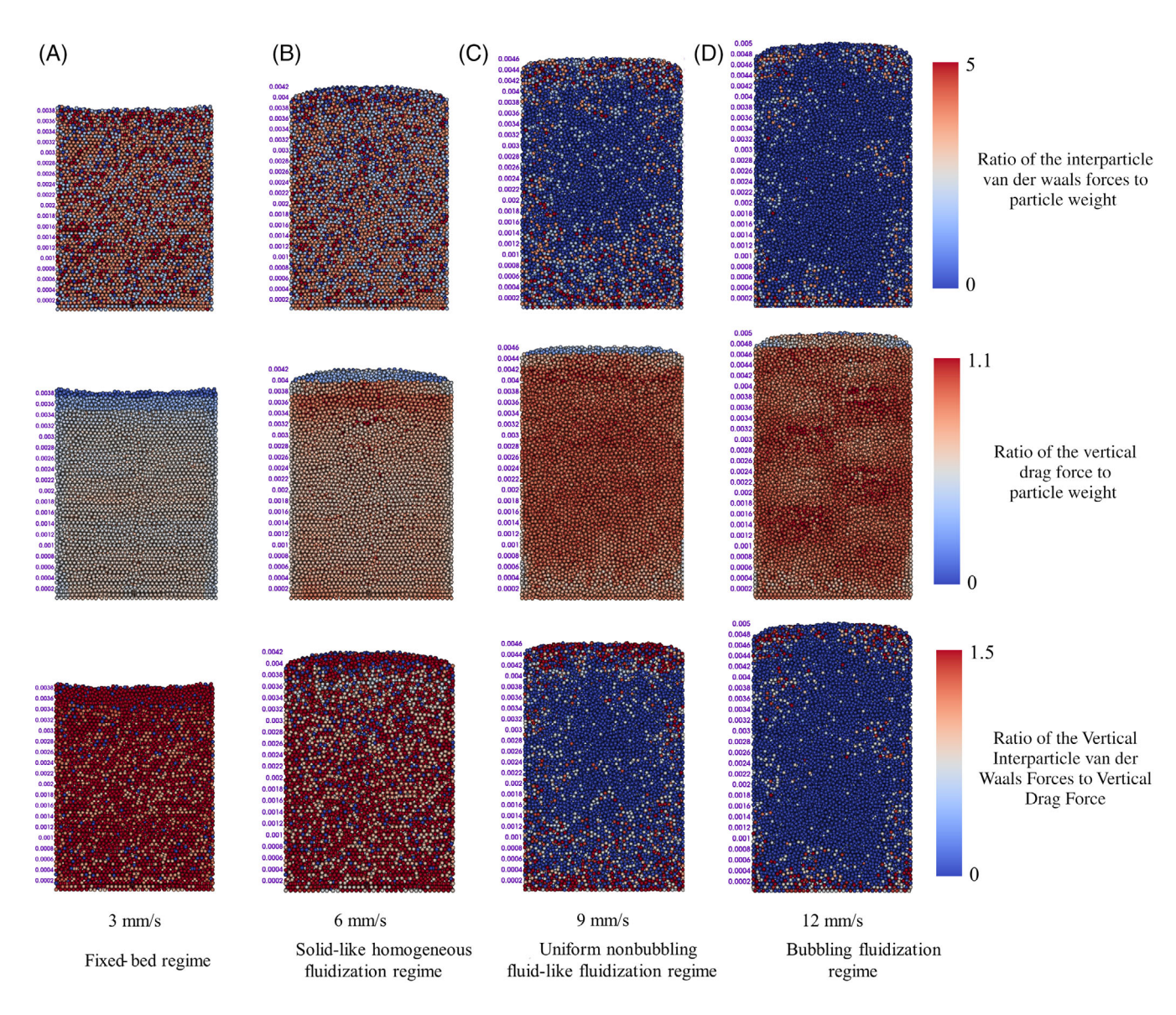


FIGURE 5 Distribution of (first row) the ratio of the interparticle van der Waals forces to particle weight, (second row) the ratio of the vertical drag force to particle weight, and (third row) the ratio of the vertical interparticle van der Waals forces to vertical drag force in the bed and at different U_g in the fluidization process

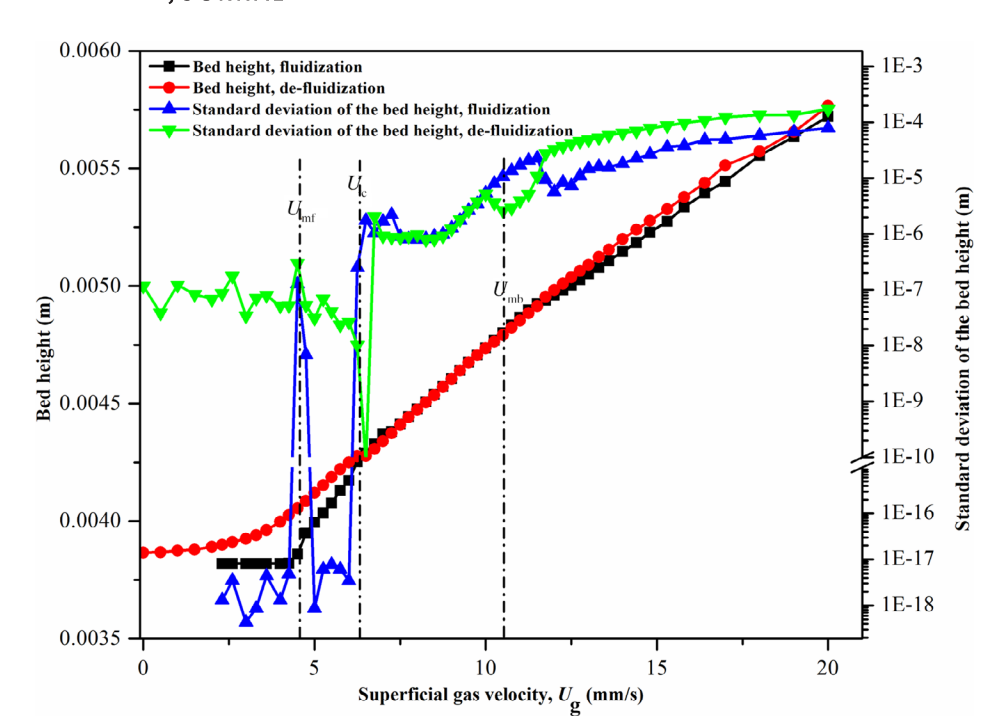


FIGURE 6 Bed height and its standard deviation against U_g in the fluidization and de-fluidization processes

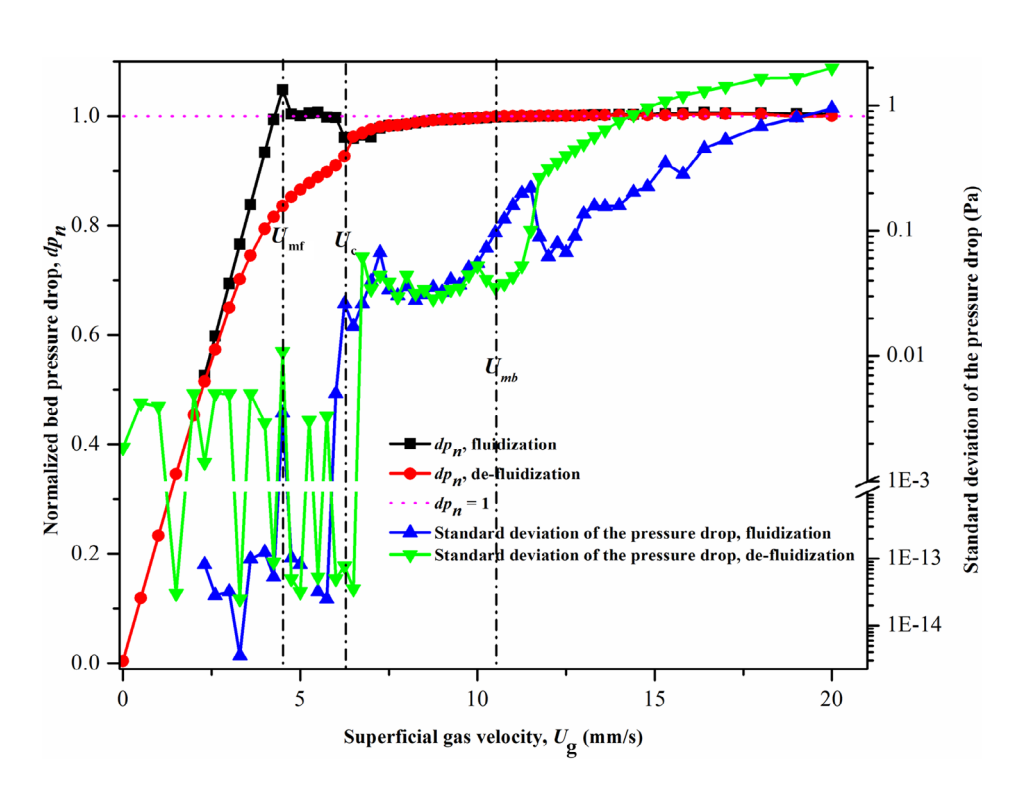


FIGURE 7 Normalized bed pressure drop and the standard deviation of the pressure drop against U_g in the fluidization and defluidization processes

drop attains a value larger than 1, that is to say, a pressure overshoot is seen. It has been found that both friction and interparticle cohesive forces are responsible for this overshoot, 20,23 as also shown later in Supporting Information Figures S6 and S8. The critical velocity between the solid-like homogeneous fluidization and uniform non-bubbling fluid-like fluidization regimes, U_c , is the first U_g at which the particles keep moving in the simulated 1.5 s; this corresponds to another spike in the standard deviation of bed height and pressure drop. Above U_c , the normalized pressure drop stabilizes around a

value of 1. $U_{\rm mb}$ is the first $U_{\rm g}$ at which obvious gas bubbles with gas void fraction larger than 0.8 appear²⁵; this is marked by a further increase in the standard deviation of pressure drop and bed height, while the bed height increases steadily and the normalized pressure drop remains constant at 1.

The following trends and demarcations are observed in the decreasing gas velocity curves: Near $U_{\rm mb}$, there is a sudden decrease in the standard deviation of bed height and pressure drop as gas velocity is decreased, while pressure drop remains constant at 1 and

bed height decreases gradually. The sudden decrease in standard deviation can be attributed to the fact that bubbles cause significant fluctuations in pressure drop and bed height. Decreasing gas velocity below $U_{\rm c}$ causes normalized pressure drop to start decreasing gradually below 1. This trend can be attributed to the fact that below U_c particle weight is no longer fully supported by drag, but rather part of it is supported by the walls and particle contacts. The standard deviation in pressure drop also decreases sharply near U_c . The bed height continues to decrease as gas velocity is decreased surrounding U_c , while the standard deviation in bed height decreases sharply near U_c . These decreases in standard deviation can be attributed to the fact that particle motion without bubbles also creates fluctuations in pressure drop and bed height, although not as significant as fluctuations produced by bubbles. As gas velocity is decreased below U_{mf} , normalized pressure drop begins to decrease more sharply, while bed height begins to decrease more gradually. The sharper decrease in pressure drop can be attributed to the fact that the bed is no longer significantly expanded in the fixed-bed state, and thus it has a lower permeability to gas flow. No significant changes in the standard deviation of bed height or pressure drop are observed in decreasing the gas velocity below $U_{\rm mf}$.

The different evolution of the bed height and normalized bed pressure drop profiles between the fluidization and de-fluidization processes can be attributed to the hysteresis effect. 5,20 Clearly in Figures 6 and 7, the hysteresis effect is only evident in the fixed-bed and solid-like homogeneous fluidization regimes, where the bed height is higher in the de-fluidization process than in the fluidization process and the normalized bed pressure drop curve during de-fluidization lies well below that for fluidization. In contrast, both the bed height and normalized bed pressure drop profiles almost coincide between the fluidization and de-fluidization processes in the uniform nonbubbling fluid-like fluidization and bubbling fluidization regimes. This occurs because in the fixed-bed and solid-like homogeneous fluidization regimes, particles have enduring and strong interparticle van der Waals forces (see Figure 5), which exert more flow resistance in the fluidization process than particles settling in the de-fluidization process. In contrast, in the uniform nonbubbling fluid-like fluidization and bubbling fluidization regimes, the interparticle van der Waals forces are no longer pronounced and particles are nearly free floating in the bed, which makes a similar flow resistance between in the fluidization and de-fluidization processes. Therefore, U_c also corresponds to the point where the hysteresis effect first appears. Although U_g is increased linearly in the CFD-DEM simulations by Galvin and Benyahia,²⁰ it is noted that their results also show a similar hysteresis effect for the bed pressure drop profile.

In total, the increasing and decreasing gas velocity curves for pressure drop, bed height and their standard deviations provide a method for demarcating between different fluidization regimes and insights into the difference in the physics of the different flow regimes.

Nevertheless, it is noted in Figure 6 that the bed height in the fluidization process increases monotonically with U_g once U_g is larger than $U_{\rm mf}$. As a result, the so-called bed contraction phenomenon in the vicinity of $U_{\rm mb}$, which is well-documented for Geldart A particles, 12,36,37 is not captured in the simulations. Wang et al. 25 attributed the failure of CFD-DEM simulations to capture the bed contraction phenomenon to the use of a small number of particles. In Wang et al..²⁵ a pseudo 2D domain was simulated, in which 2D governing equations were solved for the gas phase and 3D motion of particles were tracked. It was found that the bed contraction phenomenon near $U_{\rm mb}$ can be captured only when the number of particles is larger than 72,000. However, in the full 3D CFD-DEM simulation study by Galvin and Benyahia,²⁰ the bed contraction phenomenon was still not captured even though the number of simulated particles is larger than 90,000. Our additional simulations with increasing the bed depth to be the same as the bed width, in which the number of simulated particles is 95,830, also show a monotonic increase of bed height with U_g in the fluidization process when U_g is larger than U_{mf} (see Supporting Information Figure S4). To find the number of particles that is necessary to capture the bed contraction phenomenon in the full 3D CFD-DEM simulations, we have run extra simulations by increasing the simulated bed size and increasing the number of particles accordingly. In these simulations, only a few values of U_{σ} close to $U_{\rm mb}$ were considered to save computing time. Only a case that contained more than 200,000 particles was able to predict the bed contraction phenomenon near $U_{\rm mb}$. However, such greatly increased computing effort is quite expensive for this study, because the aim is to investigate in detail the transition between different fluidization states by increasing or decreasing $U_{\rm g}$ step-by-step and keeping the change in every adjustment small, in which many values of U_{α} need to be examined.

TABLE 3 Effect of the friction on transition velocities

μ	0	0.1	0.2	0.3
Bond number	0	0-5.6	0-5.6	0-5.6
U _{mf} (mm/s)	2.6	4	4.5	4.75
U _c (mm/s)	2.6	6.5	6.25	6.25
U _{mb} (mm/s)	9.75	10	10.5	10.75

TABLE 2 Effect of the interparticle van der Waals forces on transition velocities

A (J)	0	1×10^{-20}	2×10^{-20}	5×10^{-20}	1×10^{-19}	2×10^{-19}	5×10^{-19}
Bond number	0	0-0.6	0-1.1	0-2.8	0-5.6	0-11.2	0-28.1
U _{mf} (mm/s)	3.6	4	4	4	4.5	5	-
$U_{\rm c}$ (mm/s)	3.6	4	4.25	5.25	6.25	9.25	-
U _{mb} (mm/s)	10.25	10.25	10.25	10.25	10.5	11	-

3.2 | Effect of interparticle van der Waals forces and friction

To study the effects of interparticle van der Waals forces and friction on the range of $U_{\rm g}$ in which different regimes exist, more simulations were performed based on the base case. Note that while studying the effect of interparticle van der Waals forces, the friction coefficient was set to be the same as in the base case, and while studying the effect of friction, the Hamaker coefficient was set to be the same as in the base case. Variations in the interparticle van der Waals forces and friction may be due to different surface properties that can be caused by either different materials or by particles fluidized under different conditions, at different thermodynamic temperatures, for example. $^{3.37}$ While it is easy to turn off or on the interparticle van der Waals forces and friction and tune their magnitudes in CFD-DEM simulations, doing the same can be greatly challenging in experiments due largely to the difficulties associated with the characterization of both the interparticle van der Waals forces and friction.

Tables 2 and 3 summarize the identified transition velocities in these cases from visual inspections detailed in the last section. Furthermore, Figures S5 and S6 show equivalent plots to the fluidization curves in Figures 6 and 7, respectively, for results obtained from simulation cases with different Hamaker coefficients, and similarly, Figures S7 and S8 show results from cases with different friction coefficients. The bond number in Tables 2 and 3 (and further in Table 4) represents the value owned by at least 80% of the particles. It can be seen that when the interparticle van der Waals forces are turned off. the bed still displays an interval of homogeneous fluidization, matching previous CFD-DEM simulations of Kobayashi et al. 38 and Ye et al.²⁸ Some experimental works³⁹ also reported that there is a very short but still visible interval of homogeneous fluidization for Geldart B particles, ¹ although the interparticle van der Waals forces are generally accepted to be unimportant for this type of particles. 1,18 Furthermore, according to practical experience, $U_{\rm mb}$ is often slightly larger than $U_{\rm mf}$ for Geldart B particles in real operations.⁴⁰ We explain the existence of such a homogeneous fluidization state when the interparticle van der Waals forces are off or unimportant to the fact that a relatively small U_g is used in these states as compared to that which can create obvious bubbles. For this low value of U_g , the drag force, although it can make particles move in this state and spawn some

small voids due to particle motions, is not large enough to create as large bubbles as seen in the bubbling regime. However, without the stabilization from the interparticle van der Waals forces, the simulation results show that there is no solid-like homogeneous fluidization regime, which means $U_{\rm mf}=U_{\rm c}.$ Only when the interparticle van der Waals forces are at the similar magnitude to particle weight $(A \ge 2 \times 10^{-20} \text{ J that corresponds to the bond number of } \sim 1)$, can the solid-like homogeneous fluidization occur. These analyses address open question (2) mentioned in the Introduction section, indicating that interparticle van der Waals forces are only necessary for the solid-like homogeneous fluidization regime, but are not needed to form the uniform nonbubbling fluid-like fluidization regime. Also, to ensure the existence of the solid-like homogeneous fluidization regime, the interparticle van der Waals forces must be similar in magnitude to particle weight or greater, as seen in Table 2. With a further increase of the interparticle van der Waals forces, U_c obviously increases due to the enhanced stabilization effect from the interparticle van der Waals forces, while $U_{\rm mf}$ and $U_{\rm mb}$ only slightly increase when the interparticle van der Waals forces are sufficiently large. Therefore, the interval of solid-like homogeneous fluidization regime is widened and the interval of the uniform nonbubbling fluid-like fluidization regime is narrowed by increasing the magnitude of interparticle van der Waals forces. In the literature, the weak dependence of $U_{\rm mf}$ and $U_{\rm mb}$ on the interparticle van der Waals forces was reported by Ye et al.²³ and Wang et al.,²⁵ respectively. These qualitative analyses address open question (3) mentioned in the Introduction section regarding the effect of interparticle van der Waals forces on the transition between the solid-like and fluid-like homogeneous fluidization states. The results indicate that the transition velocity, U_c obviously increases with the increase of interparticle van der Waals forces, and unlike $U_{\rm mf}$ and $U_{\rm mb}$, $U_{\rm c}$ showing a strong dependence on interparticle van der Waals forces. When the interparticle van der Waals forces are further increased to such a value that the bond number is larger than 15 for some particles (A = 5×10^{-19} J), the bed displays the fluidization behavior of Geldart C particles, 1 showing that gas flows try to escape from the bed by forming channels. It is therefore not practical to determine the transition velocities. Such magnitude of the bond number that shows the transition between the fluidization behavior from Geldart A to Geldart C is similar to that in the work by Ye et al.²³

TABLE 4 Effect of the particle size and density on transition velocities

Particle size (μm)	75	60	90	75	75
Particle density (kg/m³)	1290	1290	1290	1100	1500
A (J)	1×10^{-19}	$5 imes 10^{-20}$	1.712×10^{-19}	$8.53 imes 10^{-20}$	1.156×10^{-19}
Bond number	0-5.6	0-5.5	0-5.6	0-5.6	0-5.6
U _{mf} (mm/s)	4.5	3	6.75	4	5
$U_{\rm c}$ (mm/s)	6.25	4.25	10.25	5.75	7.5
U _{mb} (mm/s)	10.5	9.25	12	10.5	10.75
$U_{\rm mf,c}$ (mm/s)	3.04	2.03	4.22	2.62	3.50
U _{mb,c} (mm/s)	6.96	5.57	8.35	6.96	6.96

Regarding the effect of friction, Table 3 shows that friction is necessary to fully exhibit the role of interparticle van der Waals forces in the formation of the solid-like homogeneous fluidization regime. That is to say, without either the interparticle van der Waals forces or the friction, there would be only uniform nonbubbling fluid-like fluidization regime in the homogeneous fluidization regime. Therefore, both the interparticle van der Waals forces and friction are not necessary for the existence of the uniform nonbubbling fluid-like fluidization regime, strengthening that this regime occurs due to fluid dynamic factors. $^{8-10,14}$ With the friction on and increasing the friction coefficient from 0.1 to 0.3, both the $U_{\rm mf}$ and $U_{\rm mb}$ increase, in accordance with previous conclusion draw by Galvin and Benyahia 20 and Ye et al., 23 respectively. Nevertheless, at a certain magnitude of interparticle van der Waals forces, $U_{\rm c}$ is not significantly affected by friction when the friction coefficient is increased from 0.1 to 0.3.

It should be stressed that the above insights regarding the effects of interparticle van der Waals forces and friction on the transition between the solid-like and fluid-like homogeneous states are new because this is the first study that investigates these factors.

3.3 | Effect of particle size and density

To validate the universality of the existence of the solid-like and fluidlike states for Geldart A particles in the homogeneous fluidization regime, four other Geldart A particles with varying particle size or density were also studied. Table 4 summarizes the particle properties of all the five Geldart A particles. For these simulation cases, the Hamaker coefficient was tuned such that the bond number is similar to that in the base case with the particle diameter of 75 µm and the particle density of 1290 kg/m³. For a particle with a smaller weight, the Hamaker coefficient needs to be also smaller. While it may be also easy to change the particle size and density in experiments, tuning the bond number effectively to be similar across different particles, however, is very difficult, highlighting the benefit of the current CFD-DEM simulations. The results show that for all these five Geldart A particles, both the solid-like and fluid-like states exist in the homogeneous fluidization regime, demonstrating that the analysis shown before is not a particular case for the particles studied in the base case, but should be general in the classification of Geldart A particles.

Table 4 summarizes the transition velocities between different fluidization regimes for different particles identified from visual inspections. Furthermore, Figures S9 and S10 show equivalent plots to the fluidization curves in Figures 6 and 7, respectively, for results obtained from simulation cases with different particles. Alongside the values determined from simulations, $U_{\rm mf}$ and $U_{\rm mb}$ calculated from the empirical correlations (indicated as $U_{\rm mf,c}$ and $U_{\rm mb,c}$, respectively) of Abrahamsen and Geldart, ¹⁵ as shown in Equations (17) and (18), are also included in Table 4. It can be seen that $U_{\rm mf}$ and $U_{\rm mb}$ identified from simulations are lower than those calculated from the correlations for all cases, similar to the results reported by Ye et al.²³ Nevertheless, both the simulations and the correlations show that (1) $U_{\rm mf}$ increases with the increase of particle size or particle density; (2) $U_{\rm mb}$ increases

with the increase of particle size; and (3) the particle density has no obvious effect on $U_{\rm mb}$. For $U_{\rm c}$, as a relatively new transition velocity demarcating the solid-like homogeneous fluidization and uniform non-bubbling fluid-like fluidization regimes, there is no correlation available in literature. The simulation results show that $U_{\rm c}$ increases with increasing of particle size or particle density, similar to that for $U_{\rm mf}$. These results address open question (4) mentioned in the Introduction section regarding the effects of particle size and density on $U_{\rm c}$ if the magnitude of interparticle forces normalized by particle weight is similar, which provide another new insight that has not been reported before. The similarity between $U_{\rm mf}$ and $U_{\rm c}$ may derive from the fact that $U_{\rm mf}$ indicates when the drag force overcomes the particle weight and $U_{\rm c}$ indicates when the drag force overcomes the interparticle van der Waals forces.

$$U_{\text{mf,c}} = \frac{9 \times 10^{-4} d_{\text{p}}^{1.8} \left[(\rho_{\text{p}} - \rho_{\text{g}}) \vec{\mathbf{g}} \right]^{0.934}}{\rho_{\text{p}}^{0.066} \mu_{\text{g}}^{0.87}}$$
(17)

$$U_{\text{mb,c}} = \frac{2.07 d_{\text{p}} \rho_{\text{g}}^{0.06}}{\mu_{\alpha}^{0.347}}$$
 (18)

4 | CONCLUSION

In this work, CFD-DEM simulations with the incorporation of interparticle van der Waals forces were performed for five typical Geldart A particles in a small 3D fluidized bed. By increasing U_g step-by-step and keeping the increase in each adjustment small, bed structures in the fixed-bed, homogeneous fluidization, and bubbling fluidization regimes were investigated in detail. On the basis of analyzing the change of gas void fraction, particle velocity, and granular temperature with time and analyzing the bed pressure drop and bed height hysteresis effect against U_g , it is concluded that both a solid-like and a fluid-like state exist in the homogeneous fluidization regime of Geldart A particles, which is a successful reproduction of the recent experiments. In the solid-like homogeneous fluidization regime, bed height expands compared to in the fixed bed, but the bed keeps stationary like in the fixed bed. In the uniform nonbubbling fluid-like fluidization regime, bed height further expands, and at the same time, particles keep moving, forming an overall circulation pattern. Some dynamic gas voids are also formed in the uniform nonbubbling fluidlike fluidization regime, but they are different from gas bubbles in the bubbling fluidization regime for three aspects: (1) they contain a higher volume fraction of particles, (2) they disappear quickly, and (3) their rupture at the bed surface happens in a mild manner. The force analysis indicates that the solid-like homogeneous fluidization regime is dominated by interparticle van der Waals forces, while the uniform nonbubbling fluid-like fluidization regime is dominated by drag force. The same particle dynamics and bed expansion characteristics in the solid-like homogeneous fluidization and uniform nonbubbling fluid-like fluidization regimes are also shown in the defluidization process. The transition velocities between different fluidization regimes can be identified by visual inspections or by investigating bed pressure drop and bed height and their fluctuations as gas flow is increased or decreased step-wise.

By changing the Hamaker coefficient and the friction coefficient, the effect of the interparticle van der Waals forces and friction on the range of U_g in which different regimes exist were investigated. Results show that both the interparticle van der Waals forces and friction are necessary for the existence of the solid-like homogeneous fluidization regime. Otherwise, there would be only fluid-like state in the homogeneous fluidization regime, as can be seen from the simulation results showing that fluid-like homogenous fluidization can occur without van der Waals forces or friction. Increasing the interparticle van der Waals forces has an obvious effect to increase U_c , while U_{mf} and U_{mb} are not significantly affected. Therefore, the solid-like homogeneous fluidization regime is widened and the uniform nonbubbling fluid-like fluidization is narrowed with increased interparticle van der Waals forces. But larger van der Waals forces with the bond number larger than 15 for some particles can make the bed behavior transit to Geldart C. Increasing the friction can increase $U_{\rm mf}$ and $U_{\rm mb}$, but it does not have obvious effect on U_c at the magnitude of interparticle van der Waals forces investigated here.

By changing particle size or particle density while keeping the bond number similar via tuning the Hamaker coefficient, the effects of the particle size and particle density on the transition velocities between different regimes were investigated. Results show that increasing particle size increases $U_{\rm mf}$, $U_{\rm c}$, and $U_{\rm mb}$. Increasing particle density increases $U_{\rm mf}$ and $U_{\rm c}$, but does not have a significant effect on $U_{\rm mb}$, agreeing with empirical correlations. The similarity between $U_{\rm mf}$ and $U_{\rm c}$ with the effects of particle size and particle density may derive from the fact that $U_{\rm mf}$ indicates when the drag force overcomes the particle weight and $U_{\rm c}$ indicates when the drag force overcomes the interparticle van der Waals forces.

Beyond reproducing the existence of the solid-like and fluid-like states in the homogeneous fluidization regime of Geldart A particles using CFD-DEM simulations, the benefits from CFD-DEM simulations are the capabilities to identify the effects of interparticle van der Waals forces, friction, particle size, and particle density on the transition between different fluidization regimes. Varying these parameters systematically is greatly challenging in experiments due to the difficulties associated with the characterizing and tuning the magnitude of interparticle van der Waals forces and friction experimentally. While the effects of different factors on U_{mf} and U_{mb} have been numerically studied before, for example, in Galvin and Benyahia²⁰ and Ye et al.,²³ the simulations here provide new insights on the effects of different factors on the transition velocity U_c between the solid-like and fluidlike homogeneous states. However, one drawback of this study is the small size of the bed and number of particles employed in the simulations. Therefore, one cannot expect a good quantitative agreement between the simulations and experiments, for example, as shown in Table 4. Furthermore, the well documented bed contraction phenomenon near $U_{\rm mb}$ is not captured here due to small number of particles simulated. The use of CPU-GPU cross-platform-coupled CFD-DEM, 41

for example, using the next generation of the MFiX code, MFiX-Exa, 42 which can be used to overcome the challenges of simulating millions of particles, is highlighted for potential future work to address these issues.

DATA AVAILABILITY STATEMENT

The data that support the findings of this study are available on request from the corresponding author.

ORCID

Qiang Guo https://orcid.org/0000-0002-8857-1961

Christopher M. Boyce https://orcid.org/0000-0002-6512-9118

Mao Ye https://orcid.org/0000-0002-7078-2402

REFERENCES

- Geldart D. Types of gas fluidization. *Powder Technol.* 1973;7:285-292. https://doi.org/10.1016/0032-5910(73)80037-3
- Sundaresan S. Instabilities in fluidized beds. Annu Rev Fluid Mech. 2003;35:63-88. https://doi.org/10.1146/annurev.fluid.35.101101. 161151
- Xie H-Y, Geldart D. Fluidization of FCC powders in the bubble-free regime: effect of types of gases and temperature. *Powder Technol*. 1995;82:269-277. https://doi.org/10.1016/0032-5910(94)02932-E
- Oke O, Lettieri P, Mazzei L. An investigation on the mechanics of homogeneous expansion in gas-fluidized beds. *Chem Eng Sci.* 2015; 127:95-105. https://doi.org/10.1016/j.ces.2015.01.020
- Tsinontides SC, Jackson R. The mechanics of gas fluidized beds with an interval of stable fluidization. J Fluid Mech. 1993;255:237-274. https://doi.org/10.1017/S0022112093002472
- Menon N, Durian DJ. Particle motions in a gas-fluidized bed of sand. *Phys Rev Lett.* 1997;79:3407-3410. https://doi.org/10.1103/ PhysRevLett.79.3407
- Rietema K. The effect of interparticle forces on the expansion of a homogeneous gas-fluidised bed. Chem Eng Sci. 1973;28:1493-1497. https://doi.org/10.1016/0009-2509(73)85153-X
- Cody GD, Goldfarb DJ, Storch GV, Norris AN. Particle granular temperature in gas fluidized beds. *Powder Technol.* 1996;87:211-232. https://doi.org/10.1016/0032-5910(96)03087-2
- Garg SK, Pritchett JW. Dynamics of gas-fluidized beds. J Appl Phys. 1975;46:4493-4500. https://doi.org/10.1063/1.321421
- Batchelor GK. A new theory of the instability of a uniform fluidized bed. J Fluid Mech. 1988;193:75-110. https://doi.org/10.1017/ S002211208800206X
- Valverde JM, Castellanos A, Mills P, Quintanilla MAS. Effect of particle size and interparticle force on the fluidization behavior of gasfluidized beds. *Phys Rev E*. 2003;67:051305. https://doi.org/10.1103/PhysRevE.67.051305
- Valverde JM, Quintanilla MAS, Castellanos A, Mills P. Experimental study on the dynamics of gas-fluidized beds. *Phys Rev E*. 2003;67: 016303. https://doi.org/10.1103/PhysRevE.67.016303
- Valverde JM, Castellanos A, Sanchez Quintanilla MA. Self-diffusion in a gas-fluidized bed of fine powder. *Phys Rev Lett.* 2001;86:3020-3023. https://doi.org/10.1103/PhysRevLett.86.3020
- Guo Q, Meng S, Zhao Y, et al. Experimental verification of solid-like and fluid-like states in the homogeneous fluidization regime of Geldart A particles. *Ind Eng Chem Res.* 2018;57:2670-2686. https:// doi.org/10.1021/acs.iecr.7b04559
- Abrahamsen AR, Geldart D. Behaviour of gas-fluidized beds of fine powders part I. Homogeneous Expansion. *Powder Technol.* 1980;26: 35-46. https://doi.org/10.1016/0032-5910(80)85005-4
- Liu P, LaMarche CQ, Kellogg KM, Leadley S, Hrenya CM. Cohesive grains: bridging microlevel measurements to macrolevel flow behavior

- via surface roughness. AIChE J. 2016;62:3529-3537. https://doi.org/ 10.1002/aic.15383
- LaMarche CQ, Leadley S, Liu P, Kellogg KM, Hrenya CM. Method of quantifying surface roughness for accurate adhesive force predictions. Chem Eng Sci. 2017;158:140-153. https://doi.org/10.1016/j. ces.2016.09.024
- Molerus O. Interpretation of Geldart's type A, B, C and D powders by taking into account interparticle cohesion forces. *Powder Technol.* 1982;33:81-87. https://doi.org/10.1016/0032-5910(82) 85041-9
- Garg R, Galvin J, Li T, Pannala S. Open-source MFIX-DEM software for gas-solids flows: part I-verification studies. *Powder Technol*. 2012;220:122-137. https://doi.org/10.1016/j.powtec.2011.09.019
- Galvin JE, Benyahia S. The effect of cohesive forces on the fluidization of aeratable powders. AIChE J. 2014;60:473-484. https://doi. org/10.1002/aic.14307
- Rumpf H. Particle Technology. New York, USA: Chapman and Hall; 1990
- Ding J, Gidaspow D. A bubbling fluidization model using kinetic theory of granular flow. AIChE J. 1990;36:523-538. https://doi.org/10.1002/aic.690360404
- Ye M, van der Hoef MA, Kuipers JAM. The effects of particle and gas properties on the fluidization of Geldart A particles. *Chem Eng Sci.* 2005;60:4567-4580. https://doi.org/10.1016/j.ces.2005.03.017
- Xie H-Y. The role of interparticle forces in the fluidization of fine particles. *Powder Technol.* 1997;94:99-108. https://doi.org/10.1016/S0032-5910(97)03270-1
- Wang J, van der Hoef MA, Kuipers JAM. CFD study of the minimum bubbling velocity of Geldart A particles in gas-fluidized beds. *Chem Eng Sci.* 2010;65:3772-3785. https://doi.org/10.1016/j.ces.2010. 03.023
- Duru P, Guazzelli É. Experimental investigation on the secondary instability of liquid-fluidized beds and the formation of bubbles. J Fluid Mech. 2002;470:359-382. https://doi.org/10.1017/ S0022112002002100
- Zeilstra C, Collignon JG, van der Hoef MA, Deen NG, Kuipers JAM. Experimental and numerical study of wall-induced granular convection. *Powder Technol.* 2008;184:166-176. https://doi.org/10.1016/j.powtec.2007.11.037
- Ye M, van der Hoef MA, Kuipers JAM. A numerical study of fluidization behavior of Geldart A particles using a discrete particle model. *Powder Technol.* 2004;139:129-139. https://doi.org/10.1016/j.powtec.2003.10.012
- Valverde JM, Quintanilla MAS, Castellanos A, Mills P. The settling of fine cohesive powders. EPL Europhys Lett. 2001;54:329. https://doi. org/10.1209/epl/i2001-00246-4
- Valverde JM, Castellanos A. Types of gas fluidization of cohesive granular materials. Phys Rev E. 2007;75:031306. https://doi.org/10. 1103/PhysRevE.75.031306
- Ye M, Wang J, van der Hoef MA, Kuipers JAM. Two-fluid modeling of Geldart A particles in gas-fluidized beds. *Particuology*. 2008;6:540-548. https://doi.org/10.1016/j.partic.2008.07.005

- Sande PC, Ray S. Fine mesh computational fluid dynamics study on gas-fluidization of Geldart A particles: homogeneous to bubbling bed. *Ind Eng Chem Res.* 2016;55:2623-2633. https://doi.org/10.1021/acs.iecr.5b03565
- Ozel A, Gu Y, Milioli CC, Kolehmainen J, Sundaresan S. Towards filtered drag force model for non-cohesive and cohesive particle-gas flows. *Phys Fluids*. 2017;29:103308. https://doi.org/10.1063/1.5000516
- Yu Y, Li Y, Jiang M, Zhou Q. Meso-scale drag model designed for coarse-grid Eulerian-Lagrangian simulation of gas-solid flows. Chem Eng Sci. 2020;223:115747. https://doi.org/10.1016/j.ces.2020.115747
- 35. Liu P, LaMarche CQ, Kellogg KM, Hrenya CM. Fine-particle defluidization: interaction between cohesion, Young's modulus and static bed height. *Chem Eng Sci.* 2016;145:266-278. https://doi.org/10.1016/j.ces.2016.02.024
- Simone S, Harriott P. Fluidization of fine powders with air in the particulate and the bubbling regions. *Powder Technol.* 1980;26:161-167. https://doi.org/10.1016/0032-5910(80)85059-5
- 37. Girimonte R, Formisani B. The minimum bubbling velocity of fluidized beds operating at high temperature. *Powder Technol.* 2009;189:74-81. https://doi.org/10.1016/j.powtec.2008.06.006
- Kobayashi T, Tanaka T, Kawaguchi T, Mukai T, Tsuji Y. DEM analysis on flow patterns of Geldart's group A particles in fluidized bed. J Soc Powder Technol Jpn. 2006;43:737-745. https://doi.org/10.4164/sptj. 43.737
- Loezos PN, Costamagna P, Sundaresan S. The role of contact stresses and wall friction on fluidization. *Chem Eng Sci.* 2002;57:5123-5141. https://doi.org/10.1016/S0009-2509(02)00421-9
- K. Wu, Dynamically Structured Flow in Pulsed Fluidised Beds, Cham, Switzerland: Springer International Publishing, 2021. https://doi.org/ 10.1007/978-3-030-68752-6.
- 41. He Y, Muller F, Hassanpour A, Bayly AE. A CPU-GPU cross-platform coupled CFD-DEM approach for complex particle-fluid flows. *Chem Eng Sci.* 2020;223:115712. https://doi.org/10.1016/j.ces.2020. 115712
- 42. Musser J, Almgren AS, Fullmer WD, et al. MFIX-Exa: a path toward exascale CFD-DEM simulations. *Int J High Perform Comput Appl.* Forthcoming 2021;10943420211009292. https://doi.org/10.1177/10943420211009293

SUPPORTING INFORMATION

Additional supporting information may be found in the online version of the article at the publisher's website.

How to cite this article: Guo Q, Bordbar A, Ma L, et al. A CFD-DEM study of the solid-like and fluid-like states in the homogeneous fluidization regime of Geldart A particles. *AIChE J.* 2021;e17420. doi:10.1002/aic.17420